University of Bath

Alternative formats
If you require this document in an alternative format, please contact:
openaccess@bath.ac.uk

Sulfido-Brigded 1,2-Bis(diphenylphosphino)ethane (dppe) appended Trinuclear Nickel(II) Clusters: Crystallographic and Computational Analyses

Devyani Srivastava,[a] Amita Singh,[b] Gabriele Kociok-Köhn,[c] Om Prakash,[a] Abhinav Kumar,*[a] and Mohd. Muddassir[d]

[a]Department of Chemistry, Faculty of Science, University of Lucknow, Lucknow 226 007, India.
Email: abhinavmarshal@gmail.com

[b]Department of Chemistry, Dr. Ram Manohar Lohia Avadh University, Ayodhya 224 001, India

[c]Materials and Chemical Characterisation Facility (MC^2), University of Bath, Claverton Down, Bath, BA2 7AY, UK.

[d]Department of Chemistry, College of Sciences, King Saud University, Riyadh 11451, Saudi Arabia

Abstract

The cluster compounds are still gaining considerable attention due to their peculiar behaviour and M-M bonding or M···M interactions. In this report, two sufido-bridged, 1,2-*bis*-(diphenylphosphino)ethane (dppe) appended trinuclear Ni(II) clusters having formula [Ni$_3$S$_2$(dppe)$_3$].2BPh$_4$ (**Ni$_3$S$_2$-1**) and [Ni$_3$S$_2$(dppe)$_2$(4-pyCH$_2$OH)$_2$].2PF$_6$ (**Ni$_3$S$_2$-2**) are reported. These clusters are synthesized from the same starting reactants the xanthate ligand 4-PyCH$_2$OCS$_2$Na, Ni(II) and dppe employing two different reaction pathways. The obtained compounds have been characterized by microanalyses, IR, UV-Vis, ^{1}H, ^{13}C and ^{31}P NMR spectroscopy as well as by single crystal X-ray diffraction technique. The X-ray analyses revealed that in both compounds three Ni(II) centers are coordinated to two sulfido and dppe ligands. In **Ni$_3$S$_2$-1** three dppe and two sulfido ligands are stabilising the trinuclar cluster cation while in **Ni$_3$S$_2$-2** along with two sulfido and two dppe ligands, two 4-pyCH$_2$OH are also coordinating with one of the Ni(II) center. Both **Ni$_3$S$_2$-1** and **Ni$_3$S$_2$-2** display different non-covalent interactions alongwith the Ni···Ni interactions. The nature of these interactions has been addressed with the aid of Hirshfeld surface analysis, density functional theory and quantum theory of atoms-in-molecules (QTAIM) analyses. The occurrence of such non-covalent intermolecular interactions is also well supported by the non-covalent interactions reduced density gradient (NCI-RDG) approaches. Also, the Wiberg bond index, Mayer bond

order and delocalization indices have been calculated to assess the nature of Ni···Ni interactions.

1. Introduction

The chalcogen-based ligand systems are still gaining attention due to their multifarious applications, flexible bonding and excellent π-electron delocalization behaviour. The oxygen and sulfur-based complexes of 3d transition metals are well known [1]. Amongst them, the bridging thiolate (*μ*-SR) and bridging sulfide (*μ*-S) classes have engrossed interest of crystal engineers because of their interesting coordinating behaviour and non-covalent supramolecular architectures [1]. Amongst 3d transition metal based complexes, the Ni(II) thiolate/dithiolate complexes find applications in C−S coupling reactions, hydro-desulfurization and molecular activation chemistry [1]. Also, this class of complexes are propped up with bridging dithiolate, thiosemicarbazone, and sulfido ligands to engender cubane-type structures displaying catalytic properties such as hydrogenations of aldehydes, Suzuki coupling, thio-esterification, ring cyclization reactions, and copolymerization of CO with ethylene using Ni-*μ*-SR/*μ*-S systems [1, 2]. Additionally, for photocatalytic production of H_2 from water and hydrodesulfurization, hydro-denitrogenation a variety of heterogeneous Ni−sulfide catalysts have been investigated [3]. Apart from this, Ni(II) coordinated to *μ*-S and *μ*-SR ligands find utility in CO dehydrogenase, hydrogenase, and acetyl-CoA synthetase enzymes [4a], while, *bis*(1,2-diphenylphoshinoethane) ligand and it's analogues are frequently utilized in transition-metal catalysed reactions. This is because the chelation effect resulting from this class of ligand offers advantage over monodentate ligands allows them to coordinate to numerous metal centers in bidentate manner, thereby stabilizing the associated metal complex [4b].

The thiolate/phosphide bridged trinuclear nickel sulfide clusters constitute interesting systems that have been investigated previously [5]. Apart from sulfido-/phosphorus bridging they also possess CO, cyclopentadienide, halo, and -SR moieties [6]. Further, their structural properties, coordination modes, and the nature of metal-metal bonding have been reported with interesting features. However, the electrochemical studies on these clusters are sporadically reported. A series of complexes have been synthesized by reacting MCl_2 (M = Ni or Pt) or $Pd(MeCO_2)_2$-

1,2-bis(diphenylphosphino)ethane(dppe) with NaSH or NaSeH to engender trinuclear clusters [Ni₃S₂(dppe)₃](BPh₄)₂·MeCN, [Ni₃Se₂(dppe)₃](BPh₄)₂ and **[Pd₃S₂(dppe)₃](PF₆)₂** and [Pd₃S₂(dppe)₃](PF₆)₂·MeCN and their structure and electrochemical properties were explored [5-7].

In view of the interesting properties associated with the Ni(II)-sulfido clusters, in the presented investigation, we herein report syntheses and structural characterization of two sulfido-bridged trinuclear Ni(II) clusters. Interestingly using the same starting materials/precursors, but adopting different reaction pathways two trinuclear clusters with different compositions and structures were obtained. In addition to structural characterization, the nature of different non-covalent interactions existing in the solid-state framework of these clusters have been investigated using density functional theory, NCI-RDG plots, quantum theory of atoms-in-molecules as well as Hirshfeld surface analyses. The outcomes of these entire investigations are presented herewith.
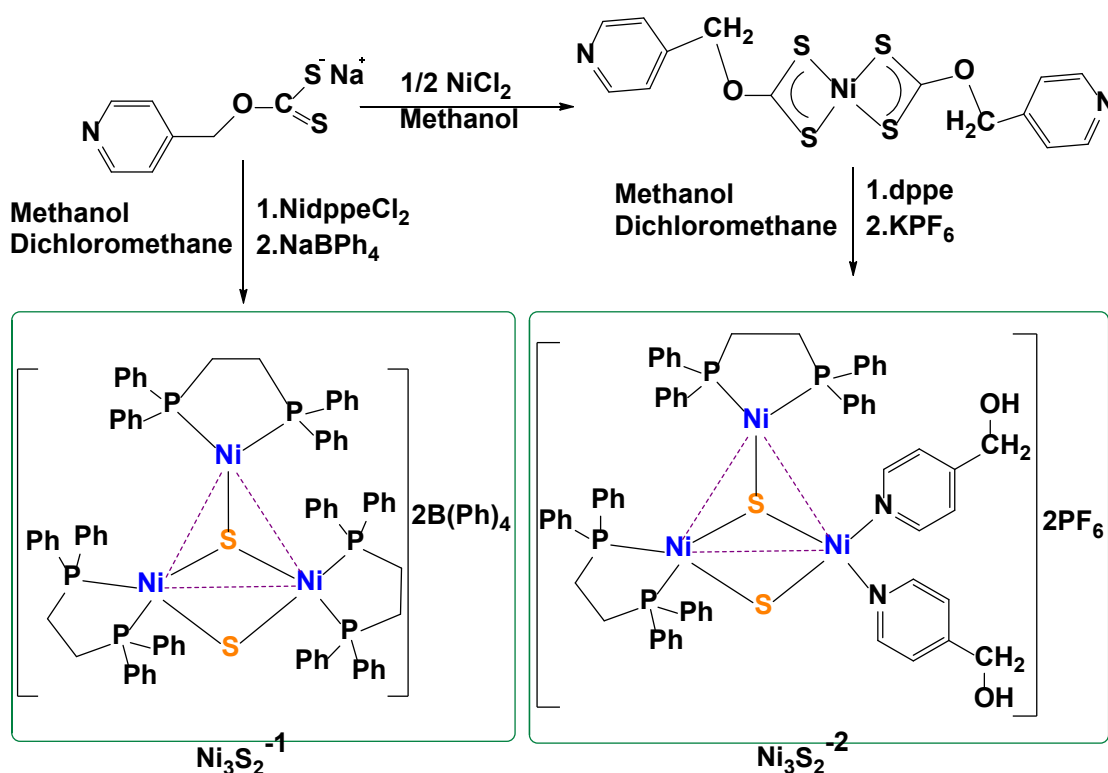
Scheme 1. Synthetic routes for the preparation of complexes.

2. Results and Discussion

2.1 Syntheses

The sulfido-bridged Ni(II) clusters were synthesized by adopting two different routes. The first method involved the reaction of 4-O-methylpyridyl xanthate ligand and NaBPh$_4$ with [NidppeCl$_2$] precursor using appropriate stoichiometric ratio in methanol and dichloromethane that yielded **Ni$_3$S$_2$-1** (Scheme 1).
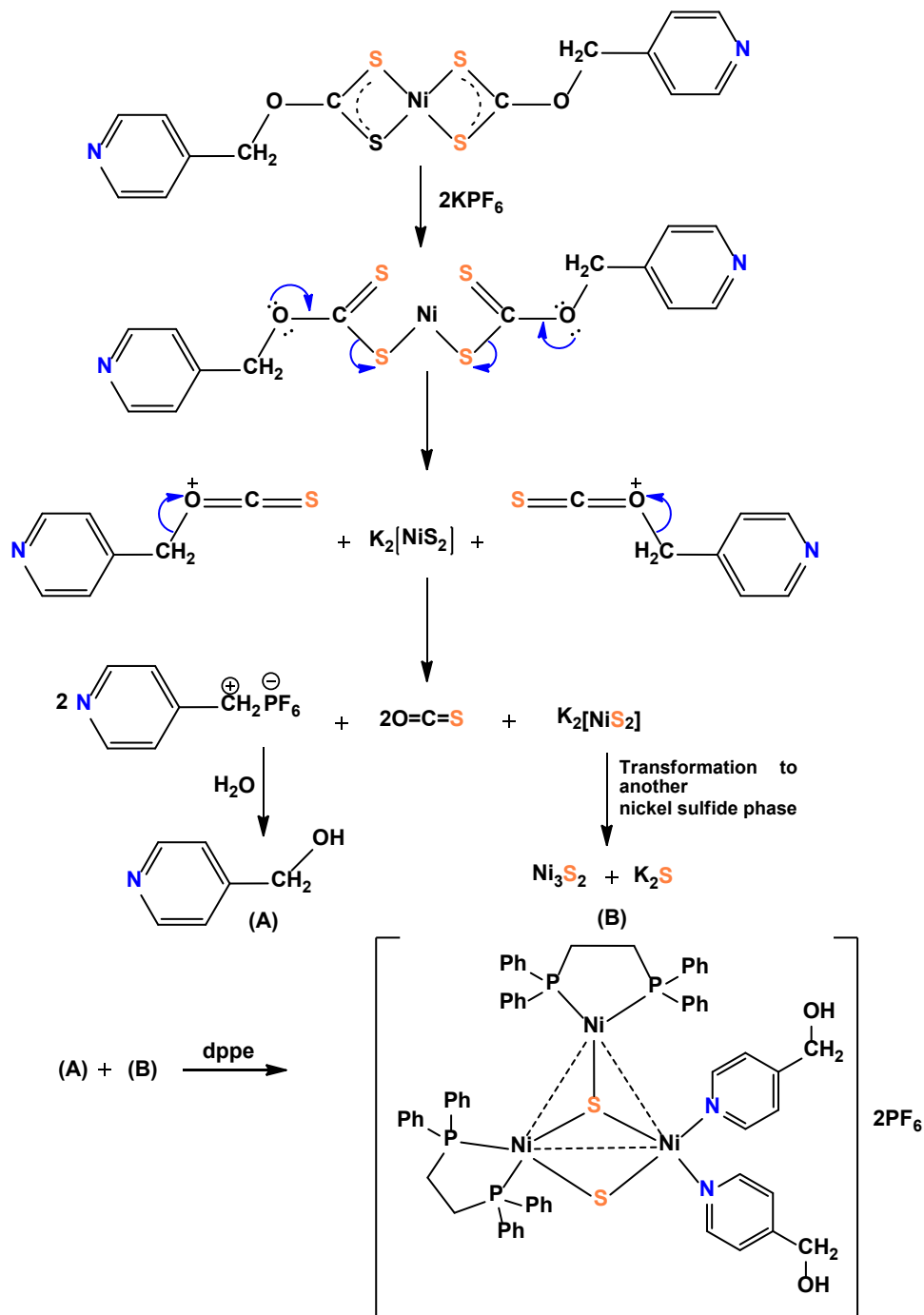
Scheme 2. Probable reaction mechanistic pathways for the formation of **Ni$_3$S$_2$-2**.

In another synthetic pathway, a homoleptic dithiolate complex was prepared by reacting NiCl$_2$.6H$_2$O with 4-O-methylpyridyl xanthate in methanol. Further, reacting

the homoleptic complex using stoichiometric quantities of dppe and KPF_6 in methanol solution yielded another Ni(II) cluster **Ni_3S_2-2**. The homoleptic di-4-O-methylpyridyl xanthatenickel(II) in presence of KPF_6 yielded 4-methylene-pyridyl carbocation, OCS and K_2NiS_2. The 4-methylene-pyridyl carbocation further was converted to 4-methylhydroxy pyridine in presence of moisture, whilst K_2NiS_2 transformed to Ni_3S_2. Both 4-methylhydroxy pyridine and Ni_3S_2 in presence of dppe ligand generated **Ni_3S_2-2** complex cation stabilized with PF_6^- (Scheme 2).

Both compounds were air stable, soluble in halogenated solvents, and insoluble in diethyl ether and petroleum ether.

2.2   Spectroscopy

In FTIR spectrum of **Ni_3S_2-1**, the bands at ~3000 and 1427 cm^{-1} are arising because of v_{C-H} and δ_{C-H}, respectively. In **Ni_3S_2-2**, the band appearing at 3361 cm^{-1} could be attributed to v_{O-H}. While, the bands appearing at 1184, 1120, 1434 and 3020 cm^{-1} could be ascribed to v_{C-O}, v_{C-N}, v_{P-C} and v_{C-H}, respectively of 4-methylhydroxy pyridine and dppe ligands. Further, to confirm the purity of both the complexes ^{1}H NMR spectroscopy was performed which revealed that in both complexes, the signals match well with the corresponding hydrogens of the dppe ligand and 4-methylhydroxy pyridine. Further, in the ^{31}P NMR spectra, the appearance of only one signal at δ 51.52 in **Ni_3S_2-1** indicated that both phosphorus centers of dppe ligand are existing in similar chemical environments. Likewise, in **Ni_3S_2-2** the resonance appearing at δ 54.52 corresponds to the phosphorus centers of dppe ligand, while the appearance of septet at δ 144.26 evinced the presence of PF_6^- counter anion [8].
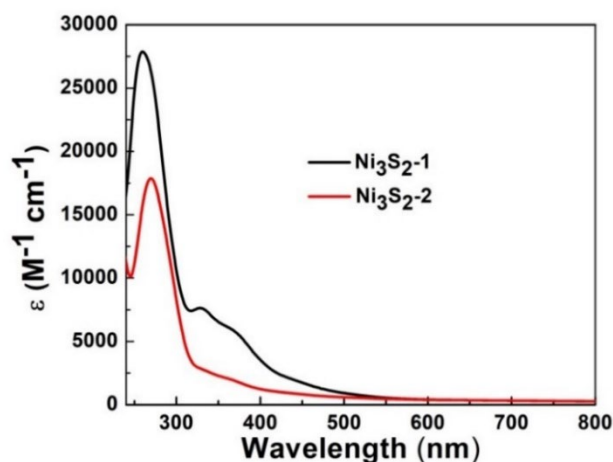

Fig. 1 Electronic absorption spectra for **Ni_3S_2-1** and **Ni_3S_2-2** recorded in 1×10^{-4} M chloroform solution.

The electronic absorption spectra for both compounds were recorded in chloroform solution (Fig. 1). For both complexes, the higher energy bands at ~260 nm are arising due to ligand-to-ligand charge transfer transitions [9]. While, bands at 330 and 367 nm in **Ni3S2-1** might be arising due to intraligand and metal to ligand charge transfer transitions, respectively [9].
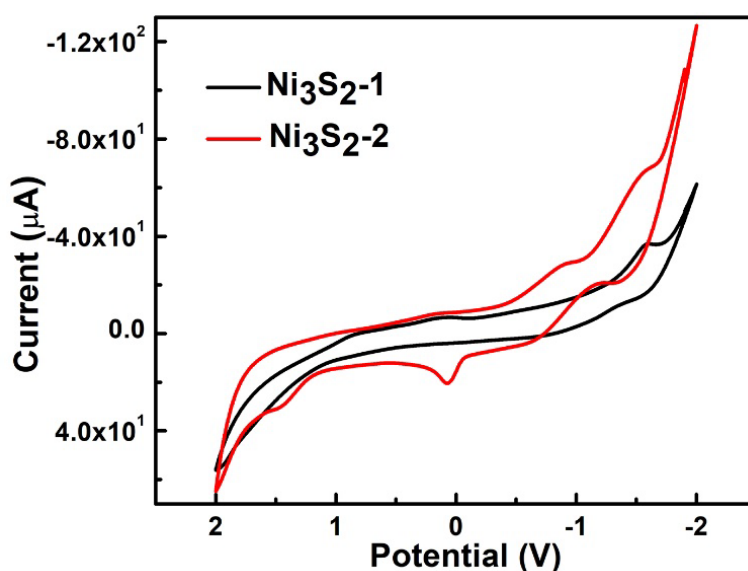
Fig. 2 Cyclic voltammograms for **Ni3S2-1** and **Ni3S2-2** recorded in 1×10^{-3} M acetonitrile solutions.

2.3   Electrochemical properties

To assess the electrochemical properties of both the compounds, cyclic voltammetry in 1×10^{-3} M acetonitrile solutions were performed using three electrode system in which a Pt disc electrode was used as the working electrode, Pt wire as a counter, and Ag/Ag^+ as reference electrode and tetra-n-butylammonium perchlorate (TBAP) as supporting electrolyte at a scan rate of 100 mV/s. In **Ni3S2-1**, one oxidation and one reduction peaks were observed at -1.6 V and -1.7 V, respectively. While, in cyclic voltammogram of **Ni3S2-2,** three oxidation peaks appeared at -1.6 V, -.0.5 V and 0.2 V while two reduction peaks appear at -1.6 V and -0.9 V [7].

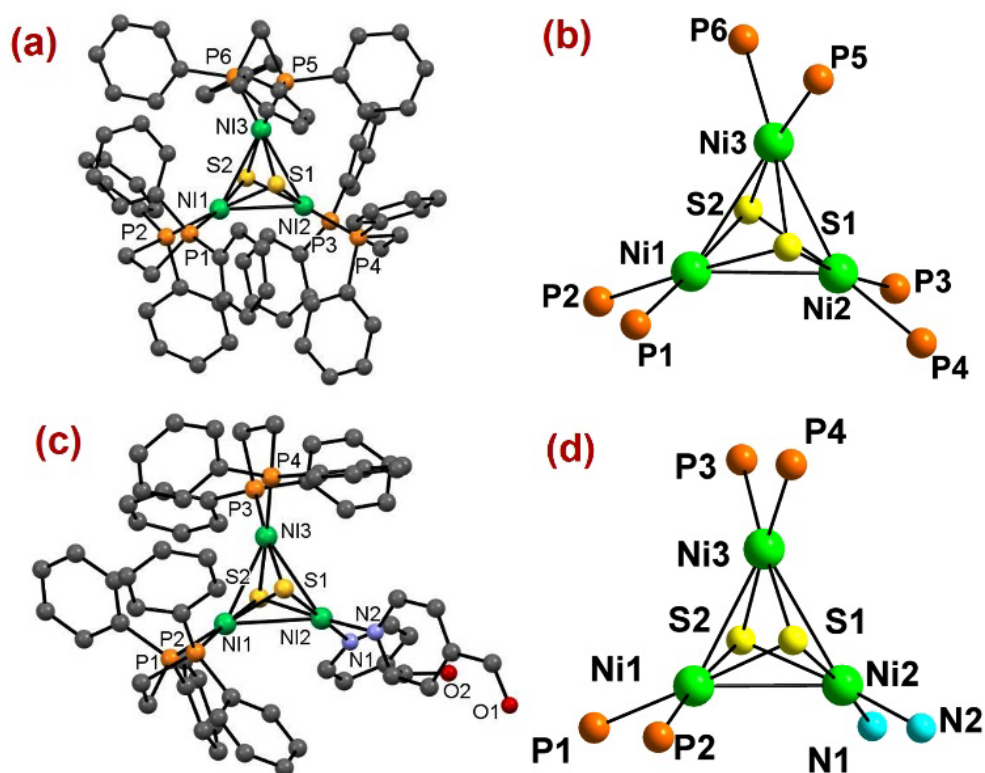**Fig. 3** Perspective view of the molecular structures of (a) and (b) **Ni$_3$S$_2$-1**; (c) and (d) **Ni$_3$S$_2$-2**. Hydrogen atoms, counter anions and co-crystallized solvent molecules have been omitted for clarity.

2.4   Molecular Structure Description

For both complexes, crystals suitable for X-ray diffraction were obtained by the layering of ethanol over chloroform solutions. The single crystal X-ray diffraction studies revealed that **Ni$_3$S$_2$-1** crystallizes in triclinic crystal system with *P*-1 space group, whereas **Ni$_3$S$_2$-2** crystallizes in monoclinic crystal system with *P*2$_1$/*c* space group. There are two molecules per unit cell in **Ni$_3$S$_2$-1**, while **Ni$_3$S$_2$-2** possesses four molecules in its unit cell. In both the compounds, inner core consist of three Ni(II) centers that form a triangular entity capped above and below by sulfur atoms. Such arrangement in both compounds gives rise to distorted trigonal pyramidal geometry [7]. However, the real geometry around each Ni(II) is distorted square planar and in **Ni$_3$S$_2$-1** this geometry is satisfied by two bridged sulfur S1 and S2 and two phosphorus centers of dppe ligand. Like **Ni$_3$S$_2$-1**, in **Ni$_3$S$_2$-2**, the distorted square planar geometries around Ni1 and Ni2 are satisfied by two sulfur and two phosphorus centers. While, the distorted square planar geometry around Ni3 is satisfied by two sulfide sulfur and two

N centers of 4-methanol pyridine. Both trinuclear Ni(II) clusters are di-cationic in nature and to counter balance the positive charge, BPh_4^- and PF_6^- anions are present in the lattices of **Ni₃S₂-1** and **Ni₃S₂-2**, respectively. In **Ni₃S₂-1**, Ni1-S1, Ni2-S1, Ni3-S1 bond lengths are 2.1918(14) Å, 2.1953(15) Å, 2.1977(14) Å whereas Ni1-S2, Ni2-S2, Ni3-S2 bond lengths are 2.2039(15) Å, 2.1965(14) Å, 2.1896(13) Å respectively. In **Ni₃S₂-2,** Ni1-S1, Ni2-S1, Ni3-S1 bond lengths are 2.193(7) Å, 2.199(7) Å, 2.166(7) Å whereas Ni1-S2, Ni2-S2, Ni3-S2 bond lengths are 2.178(6)Å, 2.205(7) Å, 2.168(6) Å respectively.

Also, the average Ni⋯Ni distances in **Ni₃S₂-1** and **Ni₃S₂-2** is 2.84 Å, which is larger than the sum of covalent radii of two nickel centers but smaller than the sum of van der Waal radii of two nickel centers ($\Sigma(Nir_{VDW})+ (Nir_{VDW}) = 3.26$ Å). Hence, the Ni⋯Ni distance parameters suggest that there is the existence of weak Ni⋯Ni interactions in both compounds. The plausible reason for the weak Ni⋯Ni interactions in both compounds is because of the diamagnetic nature of Ni(II) square planar environment [7].
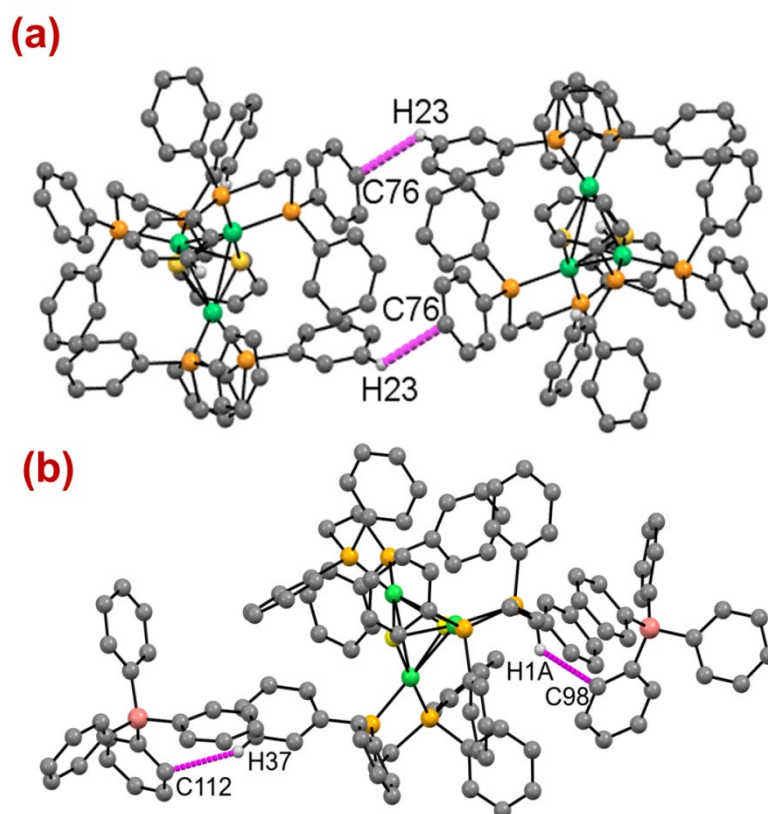

Fig. 4 (a) **Ni₃S₂-1** dimer held by C-H⋯π interactions; (b) C-H⋯π interaction between **Ni₃S₂-1** and $B(C_6H_5)_4$- anion.
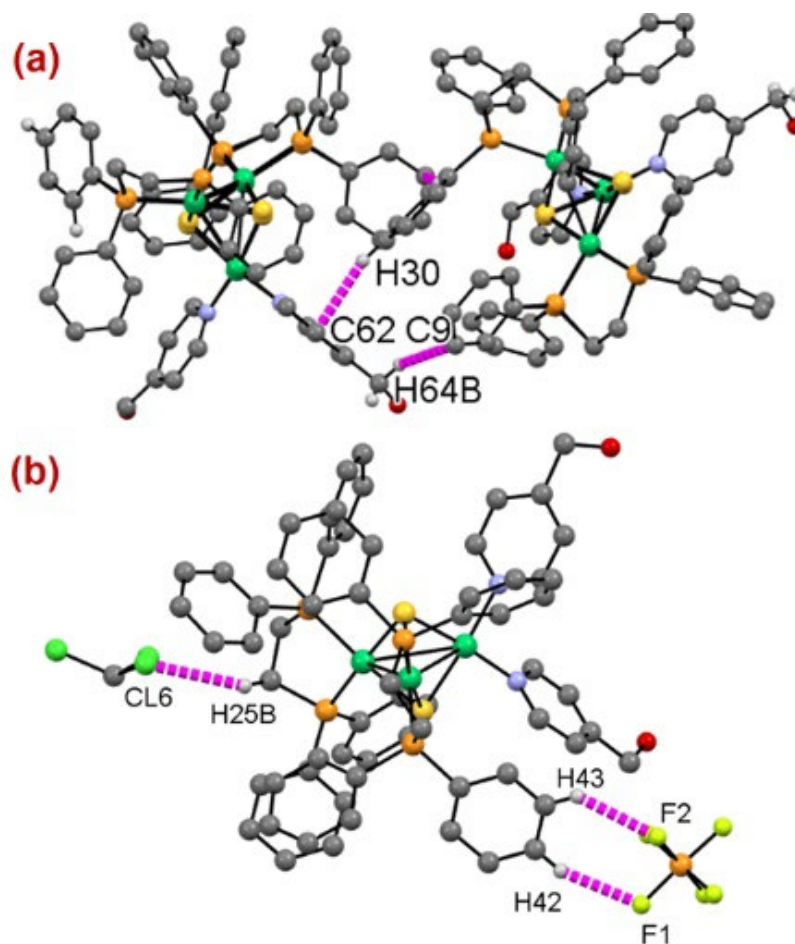
Fig. 5 (a) **Ni₃S₂-2** dimer held by C-H⋯π interactions; (b) C-H⋯Cl and C-H⋯F interaction between **Ni₃S₂-2** and CHCl₃ and PF₆ – anion, respectively.

The solid state framework in **Ni₃S₂-1** is stabilized by intermolecular C-H⋯π interactions (Fig. 4). Also, intramolecular π⋯π and C-H⋯π non covalent interactions exist between the monomer and counter anion (Fig. 4). The intermolecular C-H⋯π interaction exists between C76 of phenyl group of one dppe ligand and H23 of phenyl group of dppe ligand of another molecule with distance 2.78 Å and ∠C76⋯H23-C23 130.92°. Additionally, another intermolecular interaction occurs between aliphatic carbon C1 of dppe and H98 of aromatic ring of BPh₄⁻ while C-H⋯π operates between carbon C112 of phenyl ring of BPh₄⁻ and H37 of phenyl ring of dppe ligand. These interaction distances are 3.37 Å and 2.74 Å, respectively and the angle ∠C112⋯H37-C37 is 151.74°.

In **Ni₃S₂-2,** supramolecular architecture is stabilized by intermolecular C-H⋯π C-H⋯F and C-H⋯Cl interactions. Also, intramolecular C-H⋯π non-covalent

interactions exist in the molecule. The intermolecular C-H···π interaction exists between C21 aromatic carbon of dppe ligand and H32 hydrogen of aromatic carbon belonging to dppe ligand of another molecule with distance 2.774 Å and angle ∠C21···H32-C32 is 150.24˚. Another intermolecular C-H···π interaction operates between H64B of methylene carbon and C9 aromatic carbon of dppe ligand having length 2.79 Å with ∠C9···H64B-C64 153.32˚. The intermolecular C-H···F interactions operate between H43 and H42 centers of aromatic carbon of dppe ligand with F1 and F2 of PF_6^- counter-anion. These interactions are having distances 2.43 Å and 2.49 Å, respectively with angles 136.8˚and 160.39˚, respectively. Also, co-crystallized chloroform molecule interacts from its Cl6 with H25B hydrogen of dppe ligand with Cl···H-C distance 2.81 Å and ∠C-H···Cl 136.37˚. The intramolecular C-H···π exists between pyridyl carbon C62 and H30 of aromatic carbon of dppe with distance 2.79 Å and angle 150.24˚.

Fig. 6 Results of the Hirshfeld surface analyses for **Ni_3S_2-1**, left panel represents d_{norm}, Shape index and curvedness; central panel displays total and decomposed fingerprint plots, and right panel presents results of crystal void calculations.
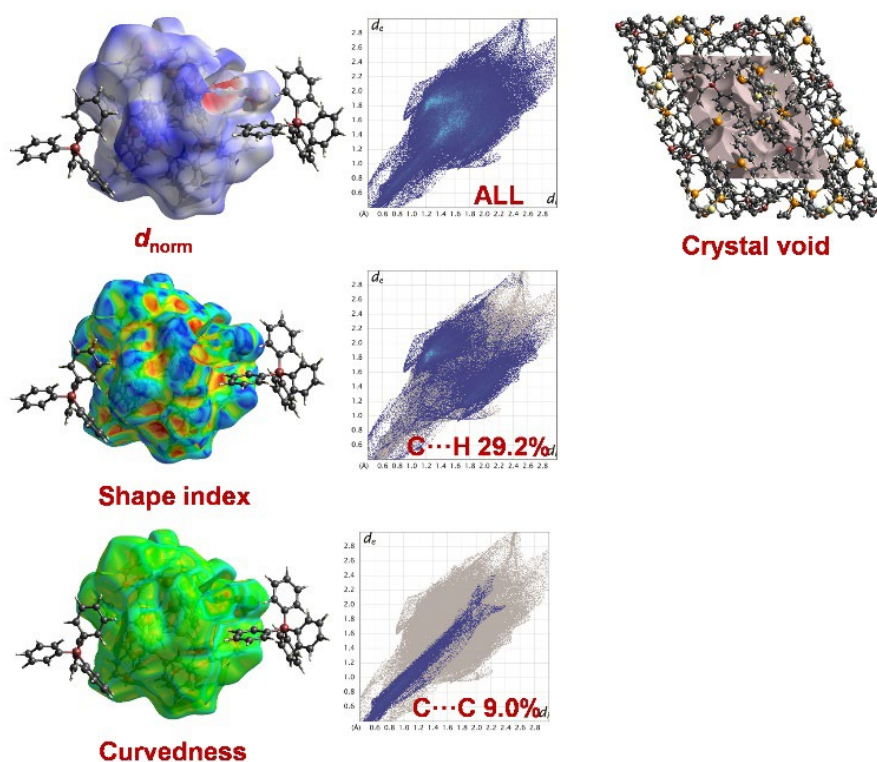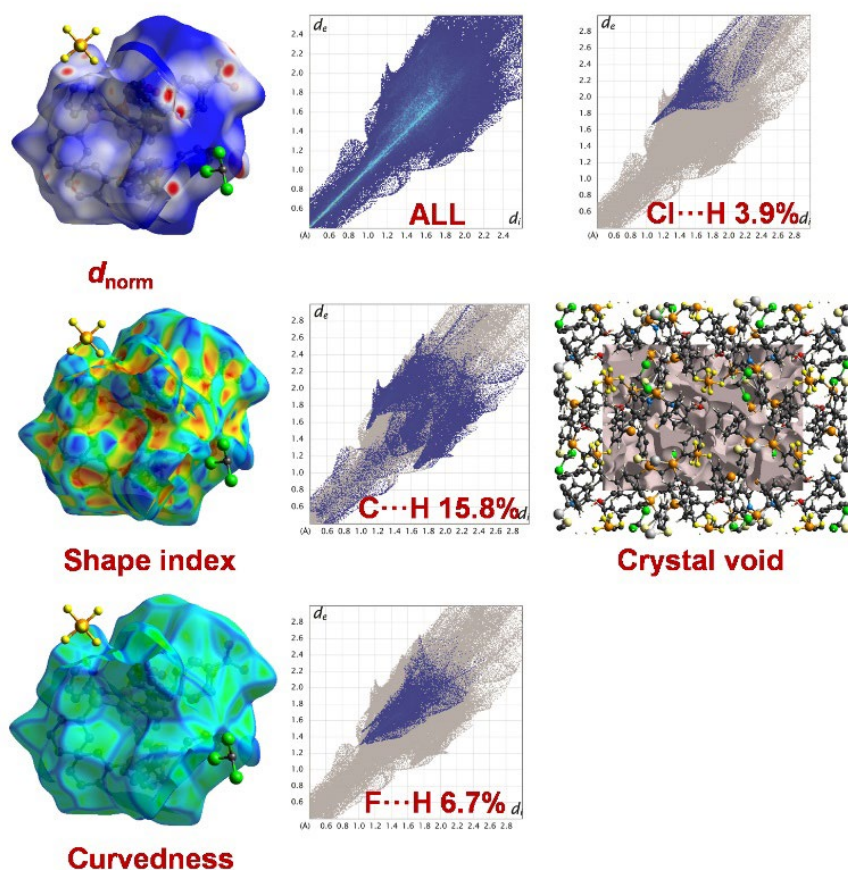
Fig. 7 Results of the Hirshfeld surface analyses for **Ni₃S₂-2**, left panel represents d_{norm}, Shape index and curvedness; central panel displays total and decomposed fingerprint plots, and right panel presents results of crystal void calculations as well as partial fingerprint plot.

2.5 Hirshfeld Surface Analyses

The Hirshfeld surfaces [10-12] for **Ni₂S₃-1** and **Ni₂S₃-2** are presented in Figures 6 and 7, respectively. The d_{norm} surfaces for both clusters are mapped over a d_{norm} range of -0.5 to 1.5 Å. Also, the surfaces are presented as transparent for the visualization of the aromatic as well as the puckered ring moieties around which they were computed. The weak non-covalent interactions as discussed in X-ray crystallography section are summarized effectively as the deep red circular depressions in the d_{norm} surfaces indicating strong non-covalent interactions. The dominant C-H⋯π and π⋯π interactions in **Ni₂S₃-1** and C-H⋯π, and Cl⋯H and F⋯H interactions in Ni₃S₂-**2** are existing in Hirshfeld surface plots as the red shaded area. Also, the small light coloured area on the surface represents weaker and longer contacts. Also, the fingerprint plots [10-12] for both the trinuclear complexes have

been constructed. In fingerprint plots, the complementary regions can be visualized where one molecule acts as a donor ($d_e > d_i$) and the other one as an acceptor ($d_e < d_i$). In **Ni₃S₂-1** The C-H⋯π interaction appears in the region 0.4 Å < ($d_e + d_i$) < 2.4 Å with 9.0% contribution as light sky-blue pattern in full fingerprint 2D plots, while, C⋯π intermolecular interaction appears between 0.4 Å < ($d_e + d_i$) < 3.4 Å with 29.2% contribution. These intermolecular interactions do not display any distinct paired spikes in their respective 2D fingerprint plots. In **Ni₃S₂-2** the C-H⋯π interactions appear as pair of spikes with central wedge between 0.4 Å < ($d_e + d_i$) < 3.0 Å with net contribution of 15.8%. The F⋯H interactions appear at the mid region of the fingerprint plot between 1.0 Å < ($d_e + d_i$) < 2.5 Å with 6.7% contribution. The peculiar feature in the fingerprint plot of **Ni₃S₂-2** is Cl⋯H interactions that exhibit single spike arising between 1.1 Å < ($d_e + d_i$) < 2.7 Å with contribution of 3.9%.

The shape index plot, which is sensitive to subtle variations in molecular shape due to irregular deformation induced from neighbouring crystalline environment, also indicates the mode of packing operating in the crystal. The bump like regions in both compounds justified weak interactions or interactions least affected by the neighbouring crystalline environment (Fig. 6 and Fig. 7). Further, the closer view of surface curvedness in **Ni₃S₂-1** indicated yellow patches within the flat green surfaces. Whilst **Ni₃S₂-2** possess blue patches with high surface curvature within the flat green surface. The yellow patches reveal the isoenergetic supramolecular interactions in **Ni₃S₂-1** (Fig. 6), but in **Ni₃S₂-2** blue patches indicate that the supramolecular interactions involved in building molecular packing in the single crystal are not iso-energetic in nature (Fig. 7).

Also, for both compounds, the crystal lattice void space has been assessed with the standard void cluster parameter "unit cell + 5.0Å" (Fig. 6 and 7). In **Ni₃S₂-1** lattice void volume was 695.41 Å³ with void area of 1736.73 Å². The complex possesses asphericity and globular indices of 0.184 and 0.219 units, respectively. For **Ni₃S₂-2**, the lattice void volume was 130.84 Å³ with void area of 2482.31 Å². The corresponding asphericity and globular indices are 0.068 and 0.233 units, respectively. The larger void volume reveals the presence of weak non-covalent interactions in the single crystal supramolecular polymer. While, small globular indices indicate that the supramolecular architectures are formed by weak non-covalent interactions in both the compounds.

2.6 Computational Insights into the weak interactions

Apart from Hirshfeld surface analyses, the weak non-covalent interaction energies in the crystal structure of both Ni_3S_2-1 and Ni_3S_2-2 have been computed using the BSSE-corrected B3LYP level of theory. The calculated interaction energies for the dimer of Ni_3S_2-1 held by C···H interactions is 7.3 kJ/mol. While the C-H···π interactions operating between Ni_3S_2-1 and two BPh_4^- counter anions possess energy of 11.7 kJ/mol. The calculated interaction energy in Ni_3S_2-2 dimer held by Ar-H···π interaction is 9.3 kJ/mol.

Table 1. Selected topographical features of intermolecular interactions computed at the B3LYP/6-31G**/CEP-121G level of theory for Ni_3S_2-1 and Ni_3S_2-2.

Bond Type	ρ_{bcp}	$\nabla^2 \rho_{bcp}$	(ε)	H	E (kJ/mol)
Ni_3S_2-1					
C76···H23	+0.0047	+0.016	+0.275	0.0009	2.62
H1A···C98	+0.0091	+0.031	--+0.403	0.0017	6.11
H37···C112	+0.0065	+0.021	+0.641	0.0011	4.01
Ni_3S_2-2					
C62···H30	+0.0055	+0.017	+.0745	0.0009	2.23
F2···H43	+0.00167	+0.009	+0.563	0.0007	2.76
Cl6···H25B	+0.0023	+0.007	+0.590	0.0004	2.25

Further, intermolecular interactions were also assessed using the Quantum Theory of Atoms in Molecules (QTAIM) analysis [14]. These calculations demonstrate the existence of bond critical points (bcp) between the interacting atomic centres, hence validating the existence of these non-covalent interactions. The electron density (bcp) between the interacting atom centres in all types of contacts, according to the QTAIM calculations, is less than +0.10 au, indicating that all of these interactions are closed shell in nature (Table 1) [14]. The positive Laplacian of the electron density (ρ_{bcp}) values for all of these interactions is further proof of the drop in electron density between these interacting atom centres (Table 1) [14]. In addition, the bond ellipticity (ε), a measure of how favourably the electron density is limited to the bond channel, revealed that none of these non-covalent interactions are cylindrically symmetrical. The overall electron energy density ($H_b = G + V$), which indicates that none of these

interactions are associated with a significant sharing of electrons, further proved the weak non-covalent character of all of these interactions [14]. Also, the interaction energies at the bond critical points were calculated using the formula $\Delta E = \frac{1}{2} V$ [14c]. The results indicated that, unlike DFT approach, the interaction energies are closer to realizations. The overestimation in energy values have been corrected to certain extent to give more reliable results as compared to that obtained with BSSE corrected interaction energies using density functional approach.
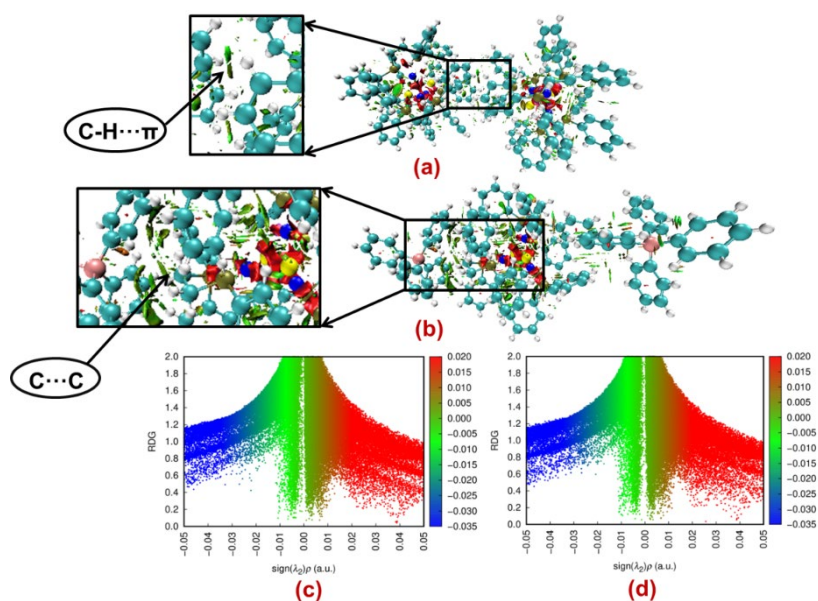

Fig. 8 3-D isosurface and 2D plots of significant non-covalent interactions for **Ni₃S₂-1** (a) and (c) between dimers (b) and (d) between monomer and counter anion.

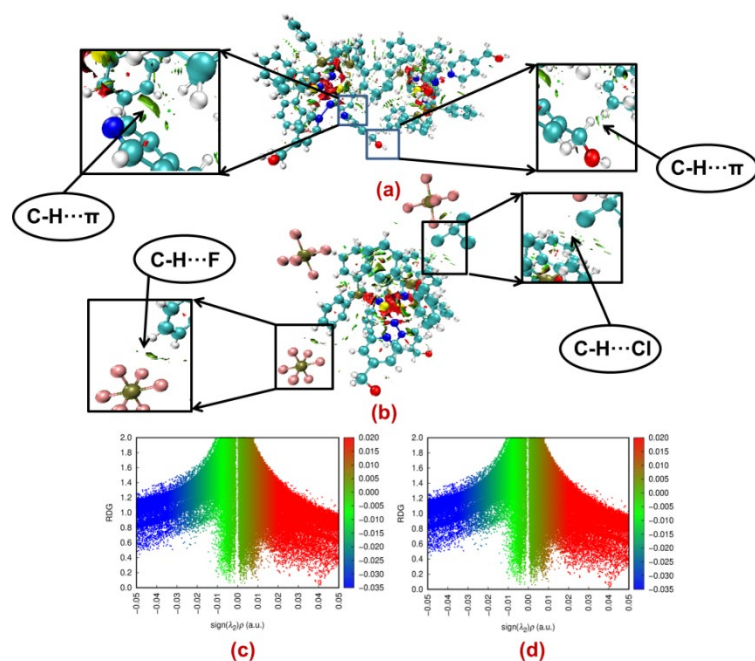**Fig. 9** 3-D isosurface and 2D plots of significant non-covalent interactions of **Ni₃S₂-2** (a) and (c) between dimers, (b) and (d) between monomer and counter anion.

2.7 NCI-RDG Analysis

NCI Plot (Non-Covalent Interactions plot) is a method for identifying and visualising non-covalent contacts such as Van der Waals interactions, hydrogen bonds, and steric conflicts [15a]. Non-covalent interactions are evidenced by regions with a small reduced density gradient and low but non-negligible density. These interactions are assessed using a visual 3D illustration using RGB (red-green-blue) colour scheme. The blue regions are associated with extremely attractive/stabilizing interactions, such as hydrogen bonding interactions. While, red regions reflect strong repulsive/destabilizing interactions, including ring closure interactions and steric interactions. The green patches, which are located between the two extremes depict weak Van der Waals interactions [15b]. The 3D isosurface plots of **Ni₃S₂-1** and **Ni₃S₂-2** are presented in Fig. 8 and Fig. 9, respectively showing significant non-covalent intermolecular interactions in the form of green patches. Also, there are some small green patches present in between the monomeric unit which are due to intramolecular interactions. Additionally, aromatic rings and triangular nickel regions have red area in the middle that demonstrated the impact of steric repulsion.

Table 2. The Ni···Ni Wiberg bond indices, Mayer Bond Orders, delocalization indices and localization indices for **Ni$_3$S$_2$-1** and **Ni$_3$S$_2$-2**.

Bond Type	Wiberg bond index	Mayer atomic bond order	Delocalization index
Ni$_3$S$_2$-1			
Ni1···Ni2	0.1263	0.0659	0.10136
Ni1···Ni3	0.1214	0.0251	0.09675
Ni3···Ni2	0.1190	0.0487	0.10069
Ni$_3$S$_2$-2			
Ni1···Ni2	0.1051	0.1000	0.10051
Ni1···Ni3	0.1163	0.0268	0.08808
Ni3···Ni2	0.1006	0.0958	0.09377

2.8   Wiberg Bond Indices, Mayer Bond Order, and Delocalization Index Calculations

Also, the nature of Ni···Ni interactions operating within both the complex cations were explored using Wiberg bond indices, Mayer bond order and delocalization index calculations. The calculations revealed that in both compounds the Wiberg bond indices obtained using natural atomic orbitals (NAOs) basis for all Ni···Ni interactions are nearly equal. Further, delocalization indices calculation that provides insight regarding the number of electrons shared or exchanged between the two atoms suggested δ(Ni,Ni) (δ = DI) are ~0.1 which suggested that there is negligible delocalization between the two atomic basins which clearly demonstrated the absence of bond between the two nickel centres [16].

3. Conclusions

In the presented investigation two sulfido-bridged, 1,2-bis(diphenylphosphino)ethane (dppe) appended trinuclear Ni(II) clusters were synthesized using the same starting reactants but adopting two different reaction pathways. Both compounds possessed three Ni(II) centers held by two sulfido-ligands and appended with dppe, but with different compositions and exhibited different non-covalent interactions alongwith the Ni···Ni interactions. Attempts were made to

address the nature of weak interactions using Hirshfeld surface analyses alongwith the DFT and AIM theory calculations. The Ni···Ni interactions observed in the X-ray structures were proved using the Wiberg bond indices, Mayer bond order and delocalization index calculations. Such investigation will upsurge interest amongst the inorganic chemists and crystal engineers to develop analogous multinuclear cluster systems that can offer peculiar structural behaviour and new M···M interactions.

4. Experimental

4.1 Materials and Methods

All chemical reagents and solvents were obtained from commercial sources and used without further purification. The chemicals 4-hydroxymethylpyridine and sodium hydride were obtained from Sigma-Aldrich and ethanol from Merck, THF, carbon disulfide, and methanol from Thermo Fischer Scientific. All solvents were distilled prior to use in accordance with previously reported standard distillation methods. The UV-Vis. spectroscopy for both compounds were performed on SPECORD 210 PLUS BU UV-Vis. spectrophotometer and elemental analyses were performed using Perkin-Elmer 2400 series II CHNS analyser. Melting points were recorded by employing open capillary method using JSGW melting point apparatus. To record IR spectra Shimadzu IR affinity 1S spectrophotometer was used, while ^{1}H, ^{13}C, and ^{31}P NMR spectra were recorded on Bruker Avance III HD spectrophotometer. Chemical shifts were reported in parts per million using TMS as an internal standard for ^{1}H and ^{13}C and phosphoric acid was used as reference for ^{31}P NMR spectroscopy. The ligand 4-PyCH$_2$OCS$_2$Na was prepared in accordance with the previously reported method [17].

4.2 Syntheses

4.2.1 Synthesis of [Ni$_3$S$_2$(dppe)$_3$].2BPh$_4$ (Ni$_3$S$_2$-1)

The ligand 4-PyCH$_2$OCS$_2$Na (0.103 g, 0.5 mmol) and NaBPh$_4$ (0.196 g, 0.5 mmol) were dissolved in dry methanol (10 mL) and stirred reaction for half an hour. To the resulting reaction mixture, NidppeCl$_2$ (0.264 g, 0.5 mmol) was added dropwise and further stirred the reaction for 60 min. The colour of the reaction mixture changed from yellow to red orange. Thereafter the reaction mixture was rotary evaporated, the residue was dissolved in dichloromethane and precipitated with diethyl ether. The final product was filtered and washed several times with diethyl ether.

Characterization data: Orange solid; yield: 0.154 g, 29.7%.; m.p. 185°C (dec). IR (KBr, cm^{-1}): 2974 (υC-H), 1427 (υP-CH$_2$).

^{1}H NMR (CDCl$_3$, 300 MHz, δ):7.60 (o-C$_6$H$_5$), 7.45(m-C$_6$H$_5$), 7.31 (p-C$_6$H$_5$), 2.51(CH$_2$-CH$_2$), ^{13}C NMR (CDCl$_3$, 75.5 MHz, δ): 134.69, 132.12, 128.94, 127.04 (-C$_6$H$_5$), 23.34 (CH$_2$-CH$_2$), ^{31}P NMR (121.54 MHz), δ: 51.52. Elemental Analysis C$_{126}$H$_{113}$B$_2$Ni$_3$P$_6$S$_2$ (%) C, 72.94; H, 5.49; S, 3.09; Found: C, 73.29; H, 5.89; S, 3.28.

4.2.2 *Synthesis of [Ni$_3$S$_2$(dppe)$_2$(4-pyCH$_2$OH)$_2$].2PF$_6$ (Ni$_3$S$_2$-2)*

To the stirring methanol solution of 4-PyCH$_2$OCS$_2$Na (0.103 g, 0.5 mmol), NiCl$_2$.6H$_2$O was added to obtain light green precipitate which was stirred for 1 hour. Thereafter, the precipitate was filtered and washed twice with methanol and air dried to obtain the homoleptic complex [Ni(4-PyCH$_2$OCS$_2$)$_2$]. The homoleptic complex [Ni(4-PyCH$_2$OCS$_2$)$_2$] (0.046 g, 0.10 mmol) was suspended in methanol (10 mL) and it was added KPF$_6$ (0.018 g, 0.1 mmol). The reaction mixture was stirred for 30 min and to it was added dichloromethane solution of 1,2-*bis*-(diphenylphosphinoethane) (0.039 g, 0.1 mmol) and this reaction mixture was stirred for 24 h. Further, the solvent was rotary evaporated and the residue was dissolved in a small amount of dichloromethane and filtered through celite and the final product was precipitated using diethyl ether.

Characterization data: Light Orange solid; yield: 0.182 g, 47.8%; m.p. 181°C. IR (KBr, cm^{-1}): 3361 (υO-H), 3020 (υC-H), 1184 (υC-O), 1120 (υC-N), 1434 (υP-CH$_2$).

^{1}H NMR (CDCl$_3$, 300 MHz, δ): 8.54 (o-NC$_5$H$_4$), 7.70 (m-NC$_5$H$_4$), 7.45 (o-C$_6$H$_5$), 7.47(m-C$_6$H$_5$), 7.49 (p-C$_6$H$_5$), 4.74 (-pyCH$_2$), 2.5 (CH$_2$-CH$_2$), ^{13}C NMR (CDCl$_3$, 75.5 MHz, δ): 132.12, 131.76, 130.83, 128.95, 21.59, ^{31}P NMR (121.54 MHz), δ: 54.52 (dppe), -144.26 (J=712Hz, PF$_6^-$). Elemental Analysis: C$_{65}$H$_{63}$Cl$_3$F$_6$N$_2$Ni$_3$O$_2$P$_5$S$_2$ (%) C, 51.37; H, 4.18; N, 1.84; S, 4.22; Found C, 51.76; H, 4.29; N, 2.06; S, 4.63.

4.3 *X-ray Crystallography*

Intensity data for **Ni$_3$S$_2$-1** and **Ni$_3$S$_2$-2** were collected at 150(2) K on a Rigaku Xcalibur, EosS2 single crystal diffractometer using graphite monochromated Mo-Kα radiation (λ = 0.71073 Å). Unit cell determination, data collection, and data reduction were performed using the CrysAlisPro software [18]. The structures were solved with SHELXT [19] and refined using full-matrix least-squares procedure based on F^2 (SHELXL-2014-16) [19]. All non-hydrogen atoms were refined anisotropically.

Hydrogen atoms were placed onto calculated positions and refined using a riding model.

Crystal data for Ni₃S₂-1: M= 2074.85 Crystal system , Triclinic, P-1, a = 14.5747(2) Å, b = 15.9109(2) Å, c = 25.2947(3) Å, α = 96.5104(11)°, β = 93.7529(10)°, γ = 113.8381(14)°, V=5290.64(13) Å^3, Z = 2, D$_{calc}$ = 1.302 Mg/m^3, F(000) = 2170, Crystal size 0.222 × 0.159 × 0.072 mm^3, Reflections collected 78464, Independent reflections 19391 [R(int) = 0.0298], GOF 1.022, Final R indices [I>2sigma(I)] R1 = 0.0873, wR2 = 0.2375, Largest diff. peak and hole 4.411 and -1.213 e.Å^{-3} **CCDC no.: 2192948.**

Crystal data for Ni₃S₂-2 C$_{65}$H$_{63}$Cl$_3$F$_6$N$_2$Ni$_3$O$_2$P$_5$S$_2$, Monoclinic, P2₁/c, a = 19.5906(7) Å, b = 16.5087(3) Å, c = 22.6614(4) Å, α = 90°, β = 90.161(2)°, γ = 90°, V = 7329.0(3) Å^3, Z = 4, D$_{calc}$ = 1.377 Mg/m^3, F(000) = 3116, Crystal size 0.366 × 0.111 × 0.091 mm^3, Reflections collected 72372, Independent reflections 14458 [R(int) = 0.0492], GOF 1.018, Final R indices [I>2sigma(I)] R1 = 0.0602, wR2 = 0.1529, Largest diff. peak and hole 0.803 and -0.724 e.Å^{-3}. **CCDC no.: 2192949**

4.4   *Computational details*

The gas phase molecular geometries of the cationic monomer as well as dimer units of both **Ni₃S₂-1** and **Ni₃S₂-2** were optimized using density functional theory (DFT) by employing the B3LYP functional [20]. For all of the atoms except Ni, 6-31G** basis set was used while for Ni CEP-121G basis set was employed. To calculate the interaction energy of the dimers held by non-covalent interactions, the interaction distances were fixed and the rest of the degrees of freedom were relaxed during geometry optimization. The stabilization energies (ΔE_{dimer}) for the dimeric entities were calculated using the formula $\Delta E_{dimer} = E_{dimer} - (2 \times E_{monomer})$ where $E_{monomer}$, E_{dimer} are the energies of the monomer and dimer entities, respectively. Since the non-covalent interactions are considerably weaker than either the ionic or covalent bonding, the basis set superposition error (BSSE) corrections were accounted for during the calculations employing the Boys-Bernardi scheme [21]. All computations have been done using the Gaussian 09 revision B.01 programme [22]. QTAIM analyses were performed using AIMALL package version 10.05.04 [23a]. The NCI-RDG analyses were performed using the Multiwfn software [23b], and the VMD

programme was used to create 3D isosurfaces [23c]. Additionally, the coloured NCI plots were created using gnuplot [23d].

4.5   *Hirshfeld Surface Analyses*

Molecular Hirshfeld surfaces in the crystal structure of both compounds were constructed by using the procedure mentioned previously [24-31].

Acknowledgement

Conflicts of interest

The authors declare no conflict of interest.

References

[1]   (a) B. Kure, A. Taniguchi, T. Nakajima, T. Tanase, Organometallics 31(2012)4791; (b) I. P. Beletskaya, V. P. Ananikov, Chem. Rev. 111(2011)1596; (c) S. Datta, D. K. Seth, R. Butcher, S. Bhattacharya, Inorg. Chim. Acta. 377(2011)120; (d) J. Torres-Nieto, W. W. Brennessel, W. D. Jones, Garcia, J. Am. Chem. Soc. 131 (2009)4120; (e) M. Ito, M. Kotera, T. Matsumoto, K. Tatsumi, Proc. Natl. Acad. Sci. U.S.A., 106(2009)11862; (f) M. V. Rampersad, E. Zuidema, J. M. Ernsting, P. W. N. M. van Leeuwen, M. Y. Darensbourg, Organometallics 26(2007)783; (g) I. Takei, Y. Wakebe, K. Suzuki, Y. Enta, T. Suzuki, Y. Mizobe, M. Hidai, Organometallics 22(2003)4639.

[2]   (a) F. Olechnowicz, G. L. Hillhouse, R. F. Jordan, Inorg. Chem. 54(2015)2705-2712; (b) S. Liu, H. Chen, H. Lv, Q.-P. Qin, L. Fan, X. Zhang, Mater. Today Chem. 24(2022)100984; (c) H. Lv, H. Chen, L. Fan, X. Zhang Inorg. Chem. 61(2022)15558–15568.

[3]   (a) C. Kong, S. Min, G. Lu, ACS Catal. 4(2014)2763; (b) O. Gutiérrez, S. Singh, E. Schachtl, J. Kim, E. Kondratieva, J. Hein, J. A. Lercher, ACS Catal. 4(2014) 1487.

[4]   (a) C. A. Ghilardi, P. Innocenti, S. Midollini, A. Orlandini, J. Chem. Soc. Dalton Trans. 1985(1985)2209; (b) H. Takano, H. Katsuyama, H. Hayashi, W. Kanna, Y. Harabuchi, S Maeda, T. Mita, Nat. Commun. 13(2022)7034.

[5]   (a) C. A. Ghilardi, S. Midollini, L. Sacconi, Inorg. Chim. Acta. 31(1978)L43; (b) F. Cecconi, C. A. Ghilardi, S. Midollini, Inorg. Chem. 22(1983)3802; (c) C. A. Ghilardi, S.

Midollini, A. Orlandini, C. Battistoni, G. Mattogno, J. Chem. Soc. Dalton Trans. 1984(1984)939.

[6]   (a) D. J. Darensbourg, D. J. Zalewski, Organometallics 3(1984)1598; (b) G. L. Simmon, L. F. Dahl, J. Am. Chem. Soc. 95(1973)2175; (c) F. Bottomle, F. Grein, Inorg. Chem. 21(1982)4170; (d) M. Hoefler, K. F. Tebbe, H. Veit, N. E. Weiler, J. Am. Chem. Soc. 105(1983)6338; (e) A. A. Pasynskii, I. L. Eremenko, B. Orazsakhatov, G. S. Gasanov, V. E. Shklover, Yu. T. Struchkov, J. Organomet. Chem. 269(1984)147; (f) A. A. Pasynskii, I. L. Eremenko, Yu. V. Rakitin, V. M. Novotortsev, O. G. Ellert, V. T. Kalinnikov, V. E. Shklover, Yu. T. Struchkov, S. V. Lindeman, T. Kh. Kurbanov, G. S. Gasanov, J. Organomet. Chem. 248(1983)309.

[7]   K. Matsumato, N. Saga, S. Tanaka, S. Ooi, J. Chem. Soc. Dalton Trans. 1991(1991)1265-1271.

[8]   R. Yadav, A. K. Singh, Y. Waghadkar, G. Kociok-Köhn, A. Kumar, R. Chauhan, S. Rane, S. Gosavi, New. J. Chem. 41(2017)1327-1333

[9]   (a) R. Chauhan, M. Trivedi, J. Singh, K. C. Molloy, G. Kociok-Köhn, U. P. Mulik, D. P. Amalnerkar, A. Kumar, Inorg. Chim. Acta, 415(2014)69-74; (b) S. P. Kaiwar, A. Vodacek, N. V. Blough, R. S. Pilato, J. Am. Chem. Soc. 119(1997)3311–3316; (c) E. G. Bakalbassis, G. A. Katsoulos, C. A. Tsipis, Inorg. Chem. 26(1987)3151–3158.

[10] (a) R. Yadav, M. Trivedi, G. Kociok-Köhn, R. Prasad, A. Kumar, CrystEngComm, 17(2015)9175-9184; (b) A. Singh, A. Singh, D. Srivastava, G. Kociok-Köhn, R. D. Köhn, A. Kumar, M. Muddassir, CrystEngComm, 24(2022)4274-4282.

[11] P. Singh, A. Singh, A. Singh, A. K. Singh, G. Kociok-Köhn, A. Alowais, N. A. Y. Abduh, M. Muddassir, A. Kumar, CrystEngComm, 22(2020)2049-2059.

[12] (a) A. Kumar, A. Singh, R. Yadav, S. Singh, G. Kociok-Köhn , M. Trivedi, Inorg. Chim. Acta 471(2018)234-243: (b) R. Yadav, M. Trivedi, R. Chauhan, R. Prasad, G. Kociok-Köhn, A. Kumar, Inorg. Chim. Acta 450(2016) 57–68; (c) M. Y. Zeng, J. Y. Chen, L. Zhang, Y. Cheng, C. Y. Lu, Y. F. Liu, A. Singh, M. Trivedi, A. Kumar, J. Q. Liu, Mater. Today Commun. 31(2022)103514

[13] C. F. Mackenzie, P. R. Spackman, D. Jayatilaka, M. A. Spackman, IUCrJ 4(2017)575–587.

[14] (a) C. F. Matta, R. J. Boyd, The Quantum Theory of Atoms in Molecules: From Solid State to DNA and Drug Design; Wiley VCH, VerlagGmbh & Co. KGaA: Germany, 2007; (b) C. F. Matta, J. Hernández-Tryjillo, T-H. Tang, R. F. W. Bader, Chem. Eur. J. 9(2003)1940-1951; (c) E. Espinosa, E. Molins, C. Lecomte, Chem. Phys. Lett. 285(1998)170.

[15]   (a) C. Chiter, A. Bouchama, T. N. Mouas, H. Allal, M. Yahiaoui, I. Warad, A. Zarrouk, A Djedouani, J. Mol. Struc. 1217(2020)128376; (b) P. Kumar, S. Banerjee, A. Radha, T. Firdoos, S. C. Sahoo, S. K. Pandey, New J. Chem. 45(2021)2249.

[16]   (a) C. Foroutan-Nejad, S. Shahbazian, R. Marek, Chem. Eur. J. 20(2014)10140; (b) S. Sowlati-Hashjinz, V. Šadek, S. Sadjadi, M. Karattunnen, A. Martin-Pendás, Nat. Commun. 13(2022)2069; (c) E. Matito, J. Poater, M. Solà M. Duran, P. Salvador, J. Phys. Chem. A 43(2005)9904–9910.

[17]   (a) A. Singh, M. Trivedi, P. Singh, G. Kociok-Köhn, U. P. Azad, A. K. Singh, A. Kumar, New J. Chem, 42(2018)18759-18764; (b) P. Singh, A. Singh, G. Kociok-Köhn, A. Kumar, M. Muddassir, Inorg. Chim. Acta 514(2021)120032; (c) X.Y. Zhang, P.K. Fu, D.Q. Xiong, Y.Y. Li, X.Y. Dong, J. Mol. Struct. 1261(2022)132889; (d) X. Z. Liu, H. P. Yang, Y. Y. Diao, Q. He, C. Y. Lu, A. Singh, A. Kumar, J. Q. Liu, Q. Lan, Chemosphere 307(2022)135729.

[18]   CrysAlisPro 1.171.40.67a, Rigaku Oxford Diffraction (2019).

[19]   (a) G. M. Sheldrick, Acta Cryst. C71(2015)3–8; (b) G. M. Sheldrick, Acta Cryst A71(2015)3-8.

[20]   (a) A.D. Becke, J. Chem. Phys. 98(1993)5648-5652; (b) C. Lee, W. Yang, R.G. Parr, Phys. Rev. B 37(1988)785-789; (c) S.H. Vosko, L. Wilk, M. Nusair, Can. J. Phys. 58(1980)1200-1211; (d) P.J. Stephens, F.J. Devlin, C.F. Chabalowski, M.J. Frisch, J. Phys. Chem. 98(1994)11623-11627.

[21]   S. F. Boys, F. Bernardi, Mol. Phys. 19(1970)553.

[22]   M. J. Frisch, G. W. Trucks, H. B. Schlegel, G. E. Scuseria, M. A. Robb, J. R. Cheeseman, J. A. Montgomery, T. Vreven Jr., K. N. Kudin, J. C. Burant, J. M. Millam, S. S. Iyengar, J. Tomasi, V. Barone, B. Mennucci, M. Cossi, G. Scalmani, N. Rega, G. A. Petersson, H. Nakatsuji, M. Hada, M. Ehara, K. Toyota, R. Fukuda, J. Hasegawa, M. Ishida, T. Nakajima, Y. Honda, O. Kitao, H. Nakai, M.; Klene, X. Li, J. E. Knox, H. P. Hratchian, J. B. Cross, V. Bakken, C. Adamo, J. Jaramillo, R. Gomperts, R. E. Stratmann, O. Yazyev, A. J. Austin, R. Cammi, C. Pomelli, J. W. Ochterski, P. Y. Ayala, K. Morokuma, G. A. Voth, P. Salvador, J. J. Dannenberg, V. G. Zakrzewski, S. Dapprich, A. D. Daniels, M. C. Strain, O. Farkas, D. K. Malick, A. D. Rabuck, K. Raghavachari, J. B. Foresman, J. V. Ortiz, Q. Cui, A. G. Baboul, S. Clifford, J. Cioslowski, B. B. Stefanov, G. Liu, A. Liashenko, P. Piskorz, I. Komaromi, R. L. Martin, D. J. Fox, T. Keith, M. A. Al-Laham, C. Y. Peng, A. Nanayakkara, M. Challacombe, P. M. W. Gill, B. Johnson, W. Chen, W. M. Wong, C. Gonzalez and J. A. Pople, Gaussian 09 revision B.01, Gaussian, Inc., Wallingford CT, 2009

[23]   (a) T.A. Keith, T. K. Gristmill Software, Overland Park KS, USA (aim.tkgristmill.com); (b) Tian Lu, Feiwu Chen, J. Comput. Chem. 33(2012)580-592; (c) W. Humphrey, A.

Dalke, K. Schulten, J. Mol. Graphics 14(1996) 33-38; (d) T. Williams, C. Kelley, Gnuplot 4.5: an interactive plotting program. URL http://gnuplot.info (2011).

[24] M. A. Spackman, J. J. McKinnon, CrystEngComm. 4(2002)378-392.

[25] M. A. Spackman, P. G. Byrom, Chem. Phy. Lett. 267(1997)309.

[26] J. J. McKinnon, A. S. Mitchell, M. A. Spackman, Chem-Eur. J. 4(1998)2136-2141.

[27] J. J. McKinnon, M. A. Spackman, A. S. Mitchell, Acta. Crystallogr. B. Struct. 60 (2004) 627-668.

[28] A. L. Rohl, M. Moret, W. Kaminsky, K. Claborn, J. J. McKinnon, B. Kahr, Cryst. Growth Des. 8(2008)4517-4525.

[29] A. Parkin, G. Barr, W. Dong, C. J. Gilmore, D. Jayatilaka, J. J. McKinnon, M. A. Spackman, C. C. Wilson, CrystEngComm 9(2007)648-652.

[30] S. K. Wolff, D. J. Greenwood, J. J. McKinnon, D. Jayatilaka, M. A. Spackman, Crystal Explorer 3.1; University of Western Australia: Perth, Australia, 2012.

[31] J. J. Koenderink, A. J. van Doorn, Image Vision Comput. 10(1992)557-564.